Exact analytical solution of the lateral spread of a particle beam in matter within a nonsmall angle limit

Seiji IKEGAMI
seiji@seiji-ikegami.org

Seiji Ikegami Research Laboratory, Orufeburu–Nagata 303, 29-1 Nisshin–dori–4chome, Chikusa–ku, Nagoya, Aichi 464-0844, Japan

Abstract
This work is the construction of an analytical theory of lateral spread within a nonsmall angle limit of an ionic or atomic beam in a target medium. The exact angular distribution theory was developed by Goudsmit and Saunderson; however, exact lateral spread model has not been constructed. Recently, ion beam cancer therapy is widely studied. Thus, the author is motivated to make a lateral spread theory involving small to large scattering angles and including the energy loss effect. The present study is successfully performed using the Bessel function, and exact analytical and numerical results are given in this text. The present research is expected to be useful for particle beam cancer treatment.

Keywords: Lateral spread, nonsmall angle limit, Thomas–Fermi–Moliere potential

1. INTRODUCTION

The present study treats a nonrelativistic energy ion beam that penetrates into an amorphous target matter. Each particle undergoes successions of elastic- and inelastic-scattering collisions. After these collisions, each particle in the beam changes its direction, resulting in beam spreading. For example, as one of expected applications of the present study, in a proton or heavy-ion beam therapy, the estimation of angular distribution and of lateral spread is needed because both are altered by collisions with the penetration depth. The energy in particle beam therapy is relativistic; however, as a basic study of interaction between particle and matter, relativistic effects are not considered in the present study. Transport equation is exactly solved in the present treatment.

A pioneering work of an angular distribution theory within a nonsmall angle limit was proposed by Goudsmit and Saunderson in the 1940s [(1), (2)]. Furthermore, within a small angle limit, Sigmund, Winterbon, and Marwick created theories for angular and lateral distributions in the 1970s [(3), (4)]. However, any lateral spread theory within nonsmall angle limit has not yet been developed. Recently, several experimental studies on carbon ion beam radiotherapy have been performed [(5) (6) (7)]. These studies have stimulated some investigators in this field to develop a more exactly treated theory on the lateral spread of a particle beam within a nonsmall angle limit. In the previous study of Ikegami [(8)], Goudsmit and Saunderson's (GS) theory has been extended from a non-energy-loss effect model to energy loss effect model. The next step is the exact construction of a lateral spread theory within a nonsmall angle limit.

Thus, the present study has aimed at the development of a new lateral spread model, and has been very well performed using the Bessel functions. An exact solution of a transport equation for the lateral spread will be shown hereafter. In the framework of a small angle limit, Marwick and Sigmund (MS) developed a lateral spread theory in 1975 [(4)]. The previous study of Ikegami [(8) (9)] introduced very well both of elastic and inelastic energy loss effects into MS's theory. The improved MS theory thus obtained is proper treatment for the energy loss effect within a small angle limit. Extent of the improved MS theory is $0.001 \leq \tau_e \leq 2000$, and the limit of MS theory must be $\rho \ll x$. The symbols τ_e, ρ and x are the reduced target thickness, lateral spread and target thickness, respectively (see Eqs. (17) and (18)). Furthermore, Liang has constructed in the 1998 a formulation of lateral range straggling by taking both elastic and inelastic energy loss effects into account [(10)]. The present theory involves the inelastic energy loss effect.

2. THEORETICAL BACKGROUND

It would be helpful for readers to survey simply the development of theoretical studies of particle-beam scattering in solid matters. Following categories may be helpful to get hold of theoretical studies reported so far:

(a) calculation within small angle limit, or within non-small angle limit

(b) calculation of angular distribution, or of lateral spread, or of both

(c) calculation taking account of energy-loss effect, or not, and if taking, inelastic, or elastic, or both

* Corresponding author. E-mail address: seiji@seiji-ikegami.org

(d) calculation using basic variables with dimension (like length, mass, charge, etc.) or using reduced variables with non-dimension

The reduced variables are non-dimensional variables that is defined in Eqs. (5, 17a, 17b, 18). The present theoretical study can be categorized as the non-small angle limit, the lateral spread and the reduced variables. Then previous papers coming under this category may be summarized simply as following way. Within small angle limit, Sigmund and Winterbon (SW) constructed the multiple scattering theory in 1974 [(3)]. In 1975, MS [(4)] developed a lateral spread theory within a small angle framework based on SW's treatment. Furthermore, with the use of reduced variables, comparisons among different projectile–target combinations for SW's and MS's theories have became possible. Valdes and Arista (VA) improved SW's theory in 1994 [(11)] by introducing the inelastic energy loss effect into SW's model. Ikegami developed in 2013 the modified VA theory by taking the elastic energy loss effect into account [(9)].

As for the theory within non-small angle limit, the first theoretical study date back to 1940 when Gaudsmit and Saunderson derived so-called GS model [(1) (2)]. Their model is useful for recent ion radiotherapy because wide-angle scattering is important for large-energy losses in the target matter. Moreover, Ikegami improved GS's theory in 2017 [(8)]. The GS–Ikegami theory involves elastic and inelastic energy loss effects.

3. THEORY

The assumptions in the present study are as follows:

(1) Target atoms are randomly and homogeneously distributed.
(2) Inelastic energy loss effect in each collision is considered.
(3) Each collision is only a binary collision with a target atom.
(4) Elastic and inelastic collisions are considered.
(5) Scaling property is held because of using the reduced variables.

The above assumptions are the same as those for the standard GS model [(1) (2)] and almost the same as those for SW's and MS's models [(3) (4)], except for the small angle limit in the latter two. Scaling property is derived by using the reduced variables that can provide a universal curve for numerical results. The present theory does not limit target thickness whether target is thick or thin, and the present treatment is involving not only small scattering angle but also large angle.

In the present investigation, the final goal is constructing Eq. (26). The ion beam initially goes along the x-axis in Fig. 1. The beam changes its direction by elastic collisions with the target atoms in the matter. The effect of inelastic collision is introduced in Eq. (20) by using VA treatment. The present lateral spread theory begins with a standard transport equation as follows:

$$F(\tilde{x}+\delta\tilde{x},\tilde{\rho}_1) = \widetilde{N}\delta\tilde{x}\int d\tilde{\sigma}(\tilde{\alpha}_2\rightarrow\tilde{\alpha}_1)\,F(\tilde{x},\tilde{\rho}_2) + \left(1-\widetilde{N}\delta\tilde{x}\int d\tilde{\sigma}(\tilde{\alpha}_1\rightarrow\tilde{\alpha}_2)\right)F(\tilde{x},\tilde{\rho}_1), \quad (1a)$$

$$-\frac{\partial}{\partial\tilde{x}}F(\tilde{x},\tilde{\rho}_1) = \widetilde{N}\int d\tilde{\sigma}\{F(\tilde{x},\tilde{\rho}_1)-F(\tilde{x},\tilde{\rho}_2)\}, \quad (1b)$$

where $F(\tilde{x},\tilde{\rho}_i)$ (i = 1,2) is the distribution function, and symbol ($\tilde{}$) means non-dimensional parameters. The quantity $\tilde{x}$ is the penetration depth in a target film, and hence $\delta\tilde{x}$ is the small penetration length in a target. In the right-hand side of Eq. (1a), the first term is the distribution with collision involving change in the lateral spread at the first angle $\tilde{\alpha}_1$ ($\tilde{\rho}_1$), and the second term is the distribution at the second angle $\tilde{\alpha}_2$ ($\tilde{\rho}_2$) without any collisions (just passing through a matter). Then, after making $\delta\tilde{x}\rightarrow 0$ in Eq. (1a), we obtain Eq. (1b). Here, $\tilde{\rho}_\phi$ is the lateral spread caused by single scattering.

Then parameters in Eqs (1a) and (1b) are described hereafter.

$$\tilde{\rho}_2 = \tilde{\rho}_1 + \tilde{\rho}_\phi. \quad (2)$$

$$\tilde{x} \equiv \frac{x}{x_{max}}\left(\frac{\beta_1}{\beta_0}\right)^{30}, \quad (3)$$

$$\tilde{\rho}_i \equiv \frac{\rho_i}{\left(\frac{x_{max}}{\beta_0}\right)} = \frac{r_i}{\left(\frac{x_{max}}{\beta_0}\right)}\sin(\alpha_i),\,(i=1,2), \quad (4)$$

$$\beta_j = \frac{E_j a_L}{2Z_1Z_2e^2},\,(j=0,1), \quad (5)$$

$$a_L = \frac{0.8853a_B}{\left(Z_1^{2/3}+Z_2^{2/3}\right)^{1/2}}, \quad (6)$$

$$\widetilde{N} \equiv Na_B^2x_{max}\left(\frac{\beta_0}{\beta_1}\right)^{30}, \quad (7)$$

and

$$d\tilde{\sigma} \equiv \frac{d\sigma}{a_B^2}. \quad (8)$$

a_L is the screening length of Lindhard et al. [(12)], and $d\sigma$ is the differential scattering cross-section derived by Lindhard and co-workers [(12)]. The non-dimensional cross section $d\tilde{\sigma}$ in Eq. (8), the non-dimensional penetration depth $\tilde{x}$ in Eq. (3), non-dimensional lateral spread $\tilde{\rho}_i$ (i = 1, 2) in Eq. (4), and the non-dimensional target atom density $\widetilde{N}$ in Eq. (7) are introduced, respectively. The parameter x_{max} is the target foil thickness, a_B is the Bohr radius, ρ_i (1, 2) is the lateral spread, r_i (1, 2) is the path length, α_i (1, 2) is the deflection angle, β_0 and β_1 are the reduced initial and the reduced final energies, E_0 and E_1 are the initial kinetic energy of projectile and the final kinetic energy of

projectile, respectively. Z_1 is the atomic number of the projectile, Z_2 is the atomic number of the target, e is the elementary charge, N is the number density of the target atoms per unit volume.
The distribution function $F(\tilde{x},\tilde{\rho}_i)$ (i = 1,2) is expressed by the Bessel function as follows:

$$F(\tilde{x},\tilde{\rho}_i) \equiv \int_0^{\tilde{x}_{max}} d\tilde{x}\, f(\tilde{x}) J_m(\tilde{x}\,\tilde{\rho}_i), (i = 1,2), \text{(9a)}$$

$$f(\tilde{x}) = \tilde{x} \int_0^{\infty} \tilde{\rho}_i d\tilde{\rho}_i\, F(\tilde{x},\tilde{\rho}_i) J_m(\tilde{x}\,\tilde{\rho}_i), (i = 1,2), \text{(9b)}$$

J_m is the m-order Bessel function of the first kind. Moreover, we use the following relations:

$$\int_0^{\infty} \tilde{\rho}_1 d\tilde{\rho}_1 J_m(\tilde{x}\,\tilde{\rho}_1) J_m(\tilde{x}'\,\tilde{\rho}_1) = \frac{1}{\tilde{x}} \delta(\tilde{x} - \tilde{x}'), \text{(10)}$$

$$J_l(\tilde{x}\,\tilde{\rho}_2) = \sum_{m=-\infty}^{\infty} J_m(\tilde{x}\,\tilde{\rho}_1) J_{l-m}\left(\tilde{x}\,\tilde{\rho}_\phi\right), \text{(11)}$$

where

J_l is the l–order Bessel function of first kind.

Using Eqs. (10) and (11) for Eqs. (2) and (3), we have the following equations:

$$\sigma(\tilde{x}) = -\tilde{x}\tilde{N} \int d\tilde{\sigma} + \tilde{N} \int d\tilde{\sigma} \int_0^{\tilde{x}_{max}} d\tilde{x} \int_0^{2\pi} d\chi \int_0^{\infty} \tilde{\rho}_\phi d\tilde{\rho}_\phi J_{l-m}\left(\tilde{x}\,\tilde{\rho}_\phi\right), \text{(13)}$$

and,

$$F(\tilde{x},\tilde{\rho}) = \mathrm{C} \int_0^{\tilde{x}_{max}} d\tilde{x}\, e^{\sigma(\tilde{x})} J_m(\tilde{x}\,\tilde{\rho}). \quad (14)$$

Here, C in the relation (14) is the initial constant for normalization. The lateral spread function $F(\tilde{x},\tilde{\rho})$ must be max at lateral spread $\tilde{\rho}$ = 0; thus, l must be 0. And then, l = 0 decides that m is 0. No summation on l and m is caused by analytical calculation process. We, consequently, regard l and m as 0.

The interatomic potential in this study is the Thomas–Fermi–Moliere potential. In accordance with Meyer's treatment [(13)], the maximum impact parameter p_{max} is defined by half the distance of neighboring atoms as:

$$p_{max} \equiv \frac{1}{2} N^{-1/3}. \quad (15)$$

Moreover, in accordance with SW's and MS's treatment [(3) (4)], new variables are introduced as in the following way because of mainly numerical reason as follows:

$$\tilde{x}\tilde{\rho} = \frac{\pi a_L^2 N x}{\pi a_L^2 N x_{max}} \left(\frac{\beta_1}{\beta_0}\right)^{30} \frac{\beta_0 \pi a_L^2 N \rho}{\pi a_L^2 N x_{max}} = \frac{\tau_e \rho_{MS}}{{\tau_{e\,max}}^2} \mu^{30}, \quad (16)$$

where

$$\tau_e = \pi a_L^2 N x \ , \quad (17a)$$

$$\tau_{e\,max} = \pi a_L^2 N x_{max}, \quad (17b)$$

$$\rho_{MS} = \beta_0 \pi a_L^2 N \rho, \quad (18)$$

and

$$\mu = \frac{\beta_1}{\beta_0}. \quad (19)$$

The quantity τ_e is the reduced penetration depth, and $\tau_{e\,max}$ is the reduced target thickness. The quantity ρ_{MS} is the reduced lateral spread, same as MS's treatment. The quantity μ is the ratio of incident and out-going energy of projectiles.

The next step is introducing the energy loss effects in accordance with VA [(11)] and Ikegami [(9)]. The basic relations for this purpose contain inelastic energy loss. Hereafter, subscripts e, indicate quantities related to the inelastic energy-loss (stopping) region. At first, the inelastic energy loss part is given by (please see Ref. [(8)]):

$$\sigma(\tilde{x}) \to \sigma_e(\tau_e) \equiv \tau_e \frac{1}{2} z_e^{1/2} \frac{G_{z_e/\mu}(\tau_e) - G_{z_e}(\tau_e)}{1 - \mu_e^{\frac{1}{2}}}, \quad (20)$$

where

$$G_{z_e}(\tau_e) \equiv \int_{z_{e\,min}}^{z_{e\,max}} dz'_e \frac{\Delta(z'_e \tau_e)}{z'^{\frac{3}{2}}_e}. \quad (21)$$

Eqs. (20) and (21) are the same of VA model [(11)]. Then, the nondimensional integration variable z_e, the reduced energy β_{0e}, and the scattering intensity parameter k are given by:

$$z_e = \frac{k}{\beta_{0e}}, \quad (22)$$

$$\beta_{0e} = \frac{E_{0e} a_L}{2 Z_1 Z_2 e^2}, \quad (23)$$

and

$$k_{min} \le k \le k_{max}, \quad (24)$$

Here, k is the scattering angle parameter affected by a single collision, and β_{0e} is the same as those in the definition of Eq. (5). E_{0e} is the projectile initial energy. As Final result, the transport cross section Δ and the lateral spread function F_e (final equation) redefined are given as following relations:

$$\Delta(z_e\tau_e) = -\int dt^{\frac{1}{2}}\frac{f\left(t^{\frac{1}{2}}\right)}{t} + \int dt^{\frac{1}{2}}\frac{f\left(t^{\frac{1}{2}}\right)}{t}\int_0^{2\pi} d\chi \int_0^{\infty} \rho_{MS\,\phi} d\rho_{MS\,\phi} J_0\left(z_e \frac{\beta_{0e}\tau_e\rho_{MS\,\phi}}{{\tau_{e\,max}}^2}\,{\mu_e}^{30}\right), \quad (25)$$

and

$$F(\tilde{x},\tilde{\rho}) \to F_e(\tau_e,\rho_{MS}) = \mathrm{C}\int_0^{\tau_{e\,max}} d\tau_e\, e^{\sigma_e(\tau_e)} J_0\left(\frac{\tau_e\rho_{MS}}{{\tau_{e\,max}}^2}\,{\mu_e}^{30}\right). \quad (26)$$

In Eqs. (25), and (26), μ_e defined by Eq. (27) is the ratios of incident and out-going energies (after passing through the target foil) for the inelastic energy loss. The quantity $\rho_{MS\,\phi}$ is the lateral spread at single collision. The parameter C is the normalized constant. The basic equations are obtained. This equation Eq. (26) is remarkable since it relates non-small angle lateral spreads in matter. Hereafter, additional explanations are mentioned for μ_e, scattering cross-section, and MS' formula.

The quantity μ_e, is described very briefly as (please see the detailed description in Ref. [(9)]:

$$\mu \to \mu_e \equiv \frac{\beta_e(\tau)}{\beta_{0e}} = \frac{E_e(\tau)}{E_{0e}} = -I_1\kappa_{ke}\tau_e + \frac{1}{2}I_2\kappa_{ke}^2\tau_e^2 + 1, \quad (27)$$

where

$$I_1 = \frac{v_i}{E_{0e}\pi a_L^2 N}, \quad (28)$$

$$I_2 = \frac{1}{mE_{0\,e}(\pi a_L^2 N)^2}, \quad (29)$$

$$\kappa_{ke} = 16\pi N(k_F a_B)\left(\frac{1}{v_B}\right)Z_1^{2/3}N_{free}A^4(m_e v_B^2 a_B^2) \times\{1-4\chi^2+\chi^4[6\ln\left(1+\frac{\pi v_F}{v_B}\right)-2\pi v_F/(\pi v_F + v_B)]\}, \quad (30)$$

$$\chi^2 = \frac{v_B}{\pi v_F}, \quad (31)$$

and

$$A = 0.56/(1-0.511Z_1^{-2/3}r_s^{-1}). \quad (32)$$

Here, v_i is the initial velocity of an incident atom, v_B is the Bohr velocity, and r_s is defined by the formula $r_s = (3/4\pi n_e)^{1/3}/a_B$. The quantity m_e is the mass of an electron. The quantity n_e is the electron density in the target matter, N_{free} is the number of free electrons per atom, k_F is the Fermi wave number, v_F is the Fermi velocity, and κ_{ke} is a constant [(14)].

It should be mentioned that Lindhard's scattering cross-section [(12)]:

$$d\sigma = \frac{\pi a_L^2}{2}\frac{dt}{t^{3/2}}f\left(t^{1/2}\right), \quad (33)$$

is valid with regard to large scattering angles,

$$t^{1/2} = \varepsilon\sin\left(\frac{1}{2}\theta_{C.M.S}\right), \quad (34)$$

$$\varepsilon = \frac{\left(\frac{m_2E}{m_1+m_2}\right)}{\left(\frac{Z_1Z_2e^2}{a_L}\right)}. \quad (35)$$

Here, $f\left(t^{1/2}\right)$ is the scattering function derived by Lindhard et al., m_1 is the mass of the projectile, and m_2 is the mass of the target atom. The quantity $\theta_{C.M.S.}$ is the angle in the center of the mass system (C.M.S.).

Moreover, if the projectile and the target atoms are the same, relation of angles between the laboratory system (L.S.) and C.M.S. is given by

$$\phi_{L.S.} = \frac{1}{2}\theta_{C.M.S.}, \quad (36)$$

and then,

$$t^{1/2} = \varepsilon\sin(\phi_{L.S.}). \quad (37)$$

Thus, we can calculate the scattering cross section $d\sigma$ as:

$$d\sigma = \pi a_L^2\frac{d(\varepsilon\sin(\phi_{L.S.}))}{\varepsilon^2\sin^2(\phi_{L.S.})}f(\varepsilon\sin(\phi_{L.S.})). \quad (38)$$

Here, $\phi_{L.S.}$ is the angle in L.S.

For comparison the lateral spread equation F_{MS} of MS model is written by [(4)]:

$$F_{MS}(\tau_e,\rho_{MS}) = \int_0^{\infty} dz_e\, z_e e^{-\tau_e/z_e\int_0^{z_e}dz_e'\Delta(z_e')}J_0\left(\frac{z_e\rho_{MS}}{\tau_e}\right), \quad (39)$$

where

$$\Delta(z_e) = \int dt^{\frac{1}{2}}\frac{f\left(t^{\frac{1}{2}}\right)}{t}\left[1-J_0\left(z_e\tilde{\phi}\right)\right], \quad (40)$$

and

$$\tilde{\phi} = \frac{E_0a_L}{2Z_1Z_2e^2}\phi = t^{\frac{1}{2}}. \quad (41)$$

4. RESULTS AND DISCUSSION

In the present study, Fortran numerical code is written by the author, and a commercial subroutine code is used. In Figs. 2–3, show examples of calculations of the lateral spread function $F_e(\tau_e, \rho_{MS})$ obtained in Eq. (26). Through all of the present figures, the collisional system calculated is for C–C; however, as a matter of fact, projectile and target are not limited to only C–C because scaling property is held by using the reduced variables. In principle, we can compare other combinations of projectile and target atoms, not only with that of C and C but also each other. In other words, the present numerical results cover any pair of collisional systems including the C–C system. Moreover, we can make comparison at any projectile energies of any collisional systems [(3) (4) (8) (9) (11)]. This is the reason why the present results are shown by using the reduced variables. Moreover, elastic energy losses effect is neglected in the present study because of a numerical problem. The numerical problem is oscillation of Bessel function, thus intensity of particle distribution of lateral spread ρ is not down in larger ρ.

Figure 2 shows variation of the lateral spread for two values of the inelastic energy–loss ratio μ_e. The values of μ_e cited are 0.9 (10% energy loss), and 0.8 (20% energy loss). The incident energy is 30 keV, the reduced thickness τ_e is 0.1 (0.85 nm), and the scattering parameter k is 1. A larger μ_e provides broader curves. A large μ_e means a big energy loss. Although the present results obtained are natural, we find that the influence of μ_e on the lateral spread is markedly large.

Figure 3 shows the comparison of $F_e(\tau_e, \rho_{MS})$ curves for three values of reduced target thickness: τ_e = 0.1 (0.85 nm), 0.15 (1.2 nm), and 0.2 (1.7 nm). The parameters adopted are k = 1, incident energy is 30 keV, and μ_e = 0.5. The present study gives calculation results that a larger τ_e provides broader lateral spreads. The number of collisions increases when the target thickness is larger. Thus, the results obtained are considered to be proper.

In the calculations shown in Figs. 2 and 3, the same value of the scattering parameter k was used. Appreciable effect k was not obtained. From a physical mathematics point of view, the k dependence (i.e., z dependence of Eq. (22)) is seen only in the transport cross section (Eq. (25)). Thus, k effect is very limited in the present model. This is the reason why k dependence was not considered in the present numerical calculations.

Figure 4 (a) shows the comparison of the present and the MS theoretical results with the experimental data [(15)]. Collisional system is O on Xe. Incident energies are 50, 60, 100, and 120 keV, and the reduced target thickness is 0.162 (1.59×10^4 nm). The results of experiments and theories are normalized to the half width of ρ. The scattering parameter k is 1.5. The present results seem to be appropriate in absolute values within the range below $E\rho \approx 2.6$. However, we cannot show the numerical results for $E\rho > 2.6$ because of a numerical problem. The numerical problem is occurrence of oscillation that is caused from Bessel function properties. The present theory involves large scattering angles in comparison with the MS's treatment within the small angle limit. In spite of this, the calculated result of the lateral spread reproduces very well the experimental results in the range below $E\rho \approx 2.6$. In the range upper $E\rho \approx 2.6$, we cut off numerical calculation because of numerical problem. Figure 4 (b) (c) show theoretical results with basic variable of ρ in atomic unit. In Fig. 4 (b), the curve of 60 keV is slightly broader than 50 keV, and in Fig. 4 (c), the curve of 120 keV also is broader than 100 keV.

Figure 5 (a), (b), (c) and (d) show the theoretical curves for τ_e = 0.1 (1.96×10^3 nm), k = 1, and collisional system is C on O (gaseous oxygen at density 1.4291 kg/m^3). Parameters of Fig. 5 (a) are 1 MeV, and μ_e = 0.7, parameters of Fig. 5 (b) are 1 MeV, and μ_e = 0.3, parameters of Fig. 5 (c) are 10 MeV, and μ_e = 0.7, and parameters of Fig. 5 (d) are 10 MeV, and μ_e = 0.7. Figure 6 (a) and (b) show the theoretical curves for τ_e = 0.1 (1.16×10^3 nm), k = 1, and collisional system C on H (gaseous hydrogen at density 0.0899 kg/m^3). Parameters of Fig. 6 (a) are 10 MeV, and μ_e = 0.7, parameters of Fig. 6 (b) are 10 MeV, and μ_e = 0.3 The tails of each curve in Figs 5 (a, b, c, d) and 6 (a ,b) are lower, but not enough because of a numerical problem. The problem is oscillation of Bessel function.

Advantages of the present results are to involve large scattering angle and to include large energy loss, even though the present study has numerical problem. Small angle approximation means that scattering angle is less than 20°, but the present treatment has no limit of angle. The present results drastically changed by the definitions of Eqs. (3, 4, 7, 8), and the future problem is to find more suitable definitions of variables.

5. CONCLUSIONS AND REMARKS

In the present study, the theoretical development has been done of an exact analytical solution of lateral spread taking the inelastic energy loss effect into account in the present model. Moreover, the effects of μ_e, and τ_e in Figs. 1, and 2, are given, respectively. The present research is expected to be useful for the ion beam radiotherapy.

ACKNOWLEDGEMENTS

I would like to thank my mentor Dr. Tetsuo NAGATA (Emeritus Professor at Meisei University, Tokyo, Japan), and I would like to thank my mentor Dr. Kazuo GODA (Emeritus Professor at Meisei University, Tokyo, Japan). I appreciate Dr. Professor Gaurav Khanna (University of Massachusetts at Dartmouth, USA) having provided the Fortran compiler gfortran. I would like to thank Dr. Neville at Enago (www.enago.jp) for the English language review.

AUTHOR CONTRIBUTION STATEMENT

The present investigation is performed by one researcher that is Seiji IKEGAMI. Other researcher do not contribute to this study.

REFERENCES

1. S. Goudsmit and J. L. Saunderson. 1940. Multiple scattering of electrons. *Phys. Rev.*, Vol. 57, p. 24. https://doi.org/10.1103/PhysRev.57.24
2. S. Goudsmit and J. L. Saunderson. 1940. Multiple scattering of electrons II. *Phys. Rev.*, Vol. 58, p. 36. https://doi.org/10.1103/PhysRev.58.36
3. P. Sigmund and K. B. Winterbon. 1974. Small-angle multiple scattering of ions in the screened coulomb region: I. angular distributions. *Nucl. Instr. and Meth.*, Vol. 119, p. 541. https://doi.org/10.1016/0029-554X(74)90805-2
4. A. D. Marwick and P. Sigmund. 1975. Small-angle multiple scattering of ions in the screened coulomb region: 2. lateral spread. *Nucl. Instr. and Meth.*, Vol. 126, p. 317. https://doi.org/10.1016/0029-554X(75)90693-X
5. K. Noda, T. Furukawa, T. Fujimoto, Y. Hara, T. Inaniwa, Y. Iwata, K. Katagiri, N. Kanematsu, K. Mizushima, S. Mori, and N. Saotome. 2017. Recent progress and future plans of heavy-ion cancer radiotherapy with HIMAC. *Nucl. Instr. and Meth. B*, Vol. 406, p. 374. https://doi.org/10.1016/j.nimb.2017.04.021
6. T. Furukawa, Y. Hara, K. Mizushima, N. Saotome, R. Tansho, Y. Saraya, T. Inaniwa, S. Mori, Y. Iwata, T. Shirai, and K. Noda. 2017. Development of NIRS pencil beam scanning system for carbon ion radiotherapy. *Nucl. Instr. and Meth. B*, Vol. 406, p. 361. https://doi.org/10.1016/j.nimb.2016.10.029
7. Y. Iwata, T. Fujimoto, S. Matsuba, T. Fujita, S. Sato, T. Furukawa, Y. Hara, K. Mizushima, Y. Saraya, R. Tansho, and N. Saotome. 2017. Recent progress of a superconducting rotating-gantry for carbon-ion radiotherapy *Nucl. Instr. and Meth. B*, Vol. 406, p. 338. https://doi.org/10.1016/j.nimb.2016.10.040
8. S. Ikegami. 2017. Extension and applications of switching model: range theory, multiple scattering model of Goudsmit–Saunderson, and lateral spread treatment of Marwick–Sigmund. *Rad. Phys. Chem.*, Vol. 138, p. 37. https://doi.org/10.1016/j.radphyschem.2017.05.002
9. S. Ikegami. 2013. Angular and lateral distributions from small angle multiple scattering including elastic and inelastic energy loss effects based on the Valdes and Arista model. *Nucl. Instr. and Meth B*, Vol. 316, p. 222. https://doi.org/10.1016/j.nimb.2013.09.019
10. J. H. Liang. 1998. Theoretical formulation for calculating lateral spread of implanted ions. *Nucl. Instr. and Meth B*, Vol. 134, p. 157. https://doi.org/10.1016/S0168-583X(98)80008-6
11. J. E. Valdés and N. R. Arista. 1994. Energy-loss effects in multiple-scattering angular distributions of ions in matter. *Phys. Rev. A*, Vol. 49, p. 2690. https://doi.org/10.1103/PhysRevA.49.2690
12. Lindhard, J., Vibeke Nielsen, and M. Scharff. 1968. Cross sections for ion-atom collisions in solids. *K. Dan. Vidensk. Selsk. Mat. Fys. Medd.*, Vol. 36, p. 10.
13. Meyer, L. 1971. Plural and multiple scattering of low-energy heavy particles in solids. *Phys. Stat. Sol. B*, Vol. 44, p. 253. https://doi.org/10.1002/pssb.2220440127
14. Kaneko, T. 1990. Energy loss and straggling of low-velocity heavy atoms in matter. *Phys. Rev. A*, Vol. 41, p. 4889. https://doi.org/10.1103/PhysRevA.41.4889
15. G. Sidenius and N. Andersen, 1975. Multiple scattering of keV ions: lateral distributions in Xenon. Nucl. Instr. And Meth, Vol. 128 p. 271.

Figure captions

Fig. 1: Geometrical explanation of lateral spread. The initial projectile direction is along the x axis. After collision, angular deviation is α and lateral spread is ρ.

Fig. 2: Comparison of the numerical results of $F_e(\tau_e, \rho_{MS})$ obtained for three values of μ_e. The parameters adopted are τ_e = 0.1 (0.85 nm); incident energy = 30 keV; and k = 1. Solid, and dotted lines correspond to μ_e = 0.9 and 0.8, respectively. Vertical and horizontal axes are the normalized intensity and the lateral spread ρ, respectively.

Fig. 3: Comparison of the numerical results of $F_e(\tau_e, \rho_{MS})$ for three values of τ_e. The parameters adopted are μ_e = 0.5; incident energy = 30 keV; and k = 1. Solid, broken, and dotted lines correspond to τ_e = 0.1 (0.85 nm), 0.15 (1.2 nm), and 0.2 (1.7 nm), respectively. Vertical and horizontal axes are the normalized intensity and the lateral spread ρ, respectively.

Fig. 4: (a) Comparison between experiment and theories for the reduced target thickness is 0.162 (1.59×10^4 nm), incident energies are 50, 60, 100, and 120 keV, collisional system is O on Xe. Vertical and horizontal axes are the normalized intensity and the lateral spread. Solid circles are experimental data, solid line is the present theory, and dotted line is MS treatment. The results of experiments and theories are normalized to the half width of ρ.
(b) Solid line is 50 keV and dotted line is 60 keV. Both of lines are theoretical results. The parameters adopted are μ_e = 0.7; and k = 0.05. Vertical and horizontal axes

are the normalized intensity and the lateral spread ρ, respectively.
(c) Solid line is 100 keV and dotted line is 120 keV. Both of lines are theoretical results. The parameters adopted are μ_e = 0.3; and k = 0.05. Vertical and horizontal axes are the normalized intensity and the lateral spread ρ, respectively.

Fig. 5 Collisional system is C on O, τ_e = 0.1 (1.96×10^3 nm) and k = 1. Solid line is theoretical carve in (a, b, c, d). Vertical and horizontal axes are the normalized intensity and the lateral spread ρ, respectively.
(a) Projectile energy is 1 MeV, and μ_e = 0.7.
(b) Projectile energy is 1 MeV, and μ_e = 0.3.
(c) Projectile energy is 10 MeV, and μ_e = 0.7.
(d) Projectile energy is 10 MeV, and μ_e = 0.3.

Fig. 6 Collisional system is C on H, τ_e = 0.1 (1.16×10^3 nm) and k = 1. Solid line is theoretical curve in (a, b). Vertical and horizontal axes are the normalized intensity and the lateral spread ρ, respectively.
(a) Projectile energy is 10 MeV, and μ_e = 0.7.
(b) Projectile energy is 10 MeV, and μ_e = 0.3.

Fig. 1

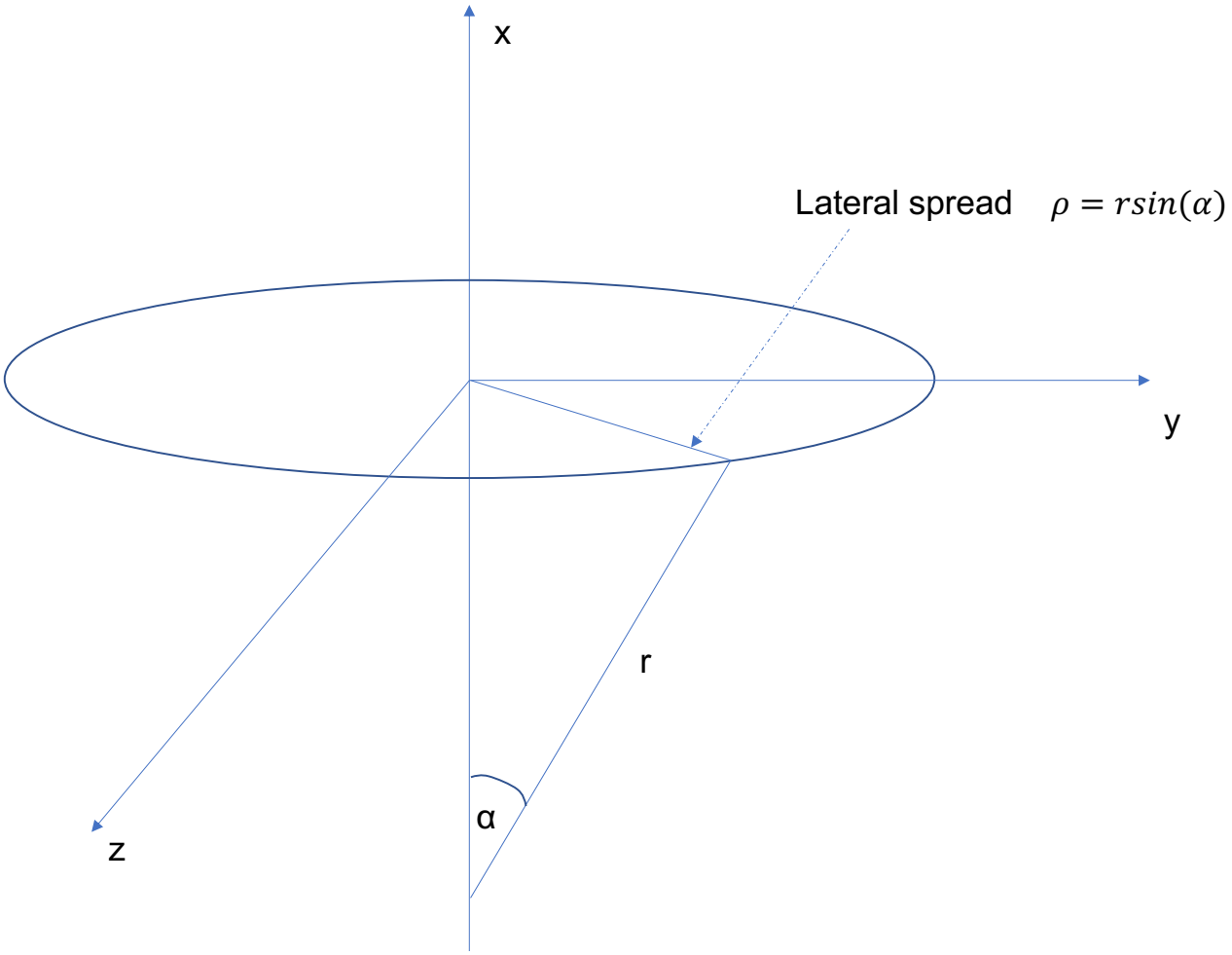

Fig.2

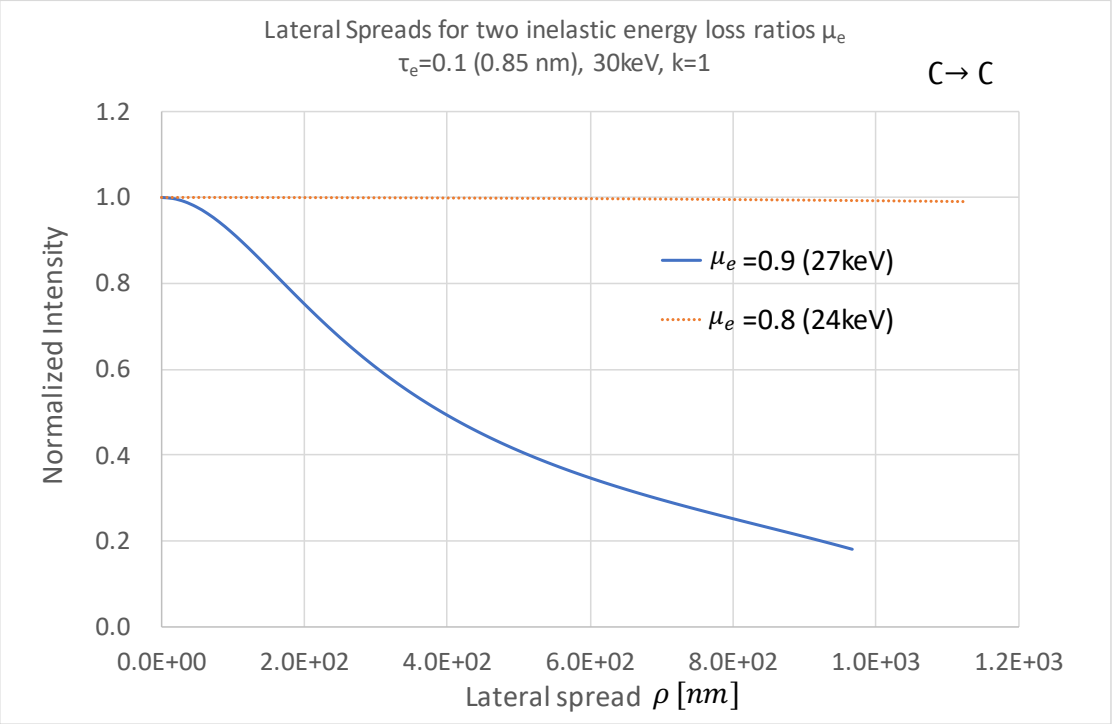
Lateral Spreads for two inelastic energy loss ratios μe
τe=0.1 (0.85 nm), 30keV, k=1
C→ C
Normalized Intensity
1.2
1.0
0.8
0.6
0.4
0.2
0.0
0.0E+00
2.0E+02
4.0E+02
6.0E+02
8.0E+02
1.0E+03
1.2E+03
Lateral spread ρ [nm]
μe =0.9 (27keV)
μe =0.8 (24keV)

Fig.3

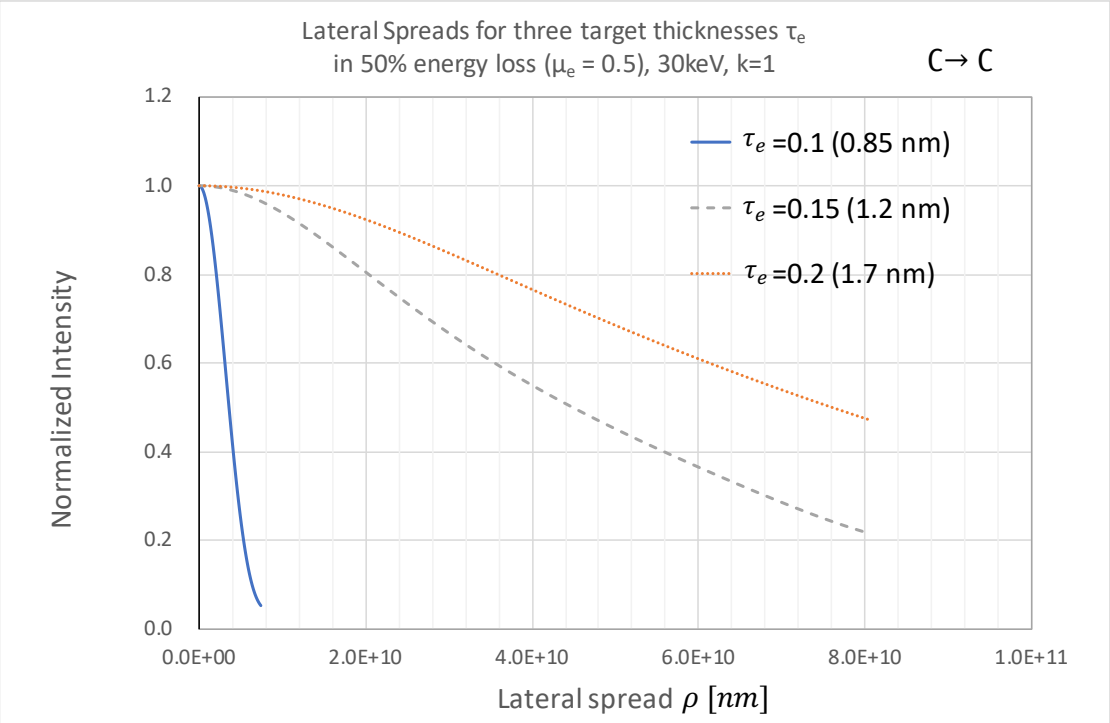
Lateral Spreads for three target thicknesses τe
in 50% energy loss (μe = 0.5), 30keV, k=1
C→ C
τe =0.1 (0.85 nm)
τe =0.15 (1.2 nm)
τe =0.2 (1.7 nm)
Normalized Intensity
1.2
1.0
0.8
0.6
0.4
0.2
0.0
0.0E+00
2.0E+10
4.0E+10
6.0E+10
8.0E+10
1.0E+11
Lateral spread ρ [nm]

Fig.4 (a)

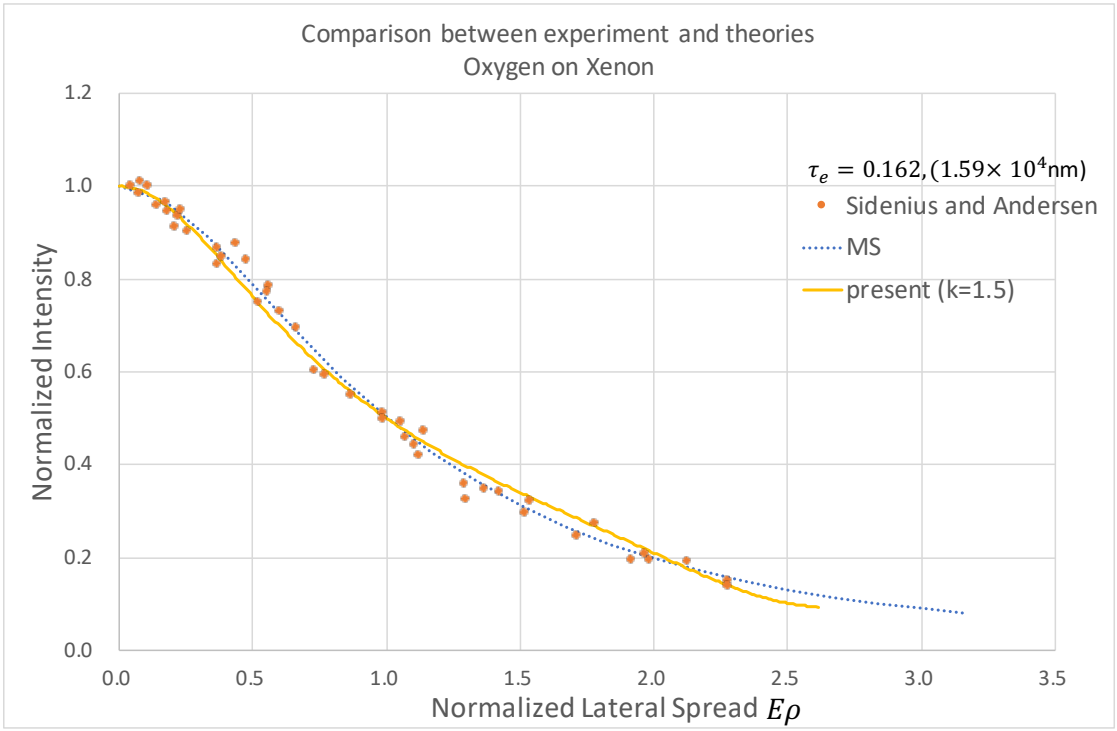
Comparison between experiment and theories
Oxygen on Xenon
Normalized Intensity
Normalized Lateral Spread $E\rho$
$\tau_e = 0.162, (1.59\times 10^4 \text{nm})$
Sidenius and Andersen
MS
present (k=1.5)
1.2
1.0
0.8
0.6
0.4
0.2
0.0
0.0
0.5
1.0
1.5
2.0
2.5
3.0
3.5

Fig.4 (b)

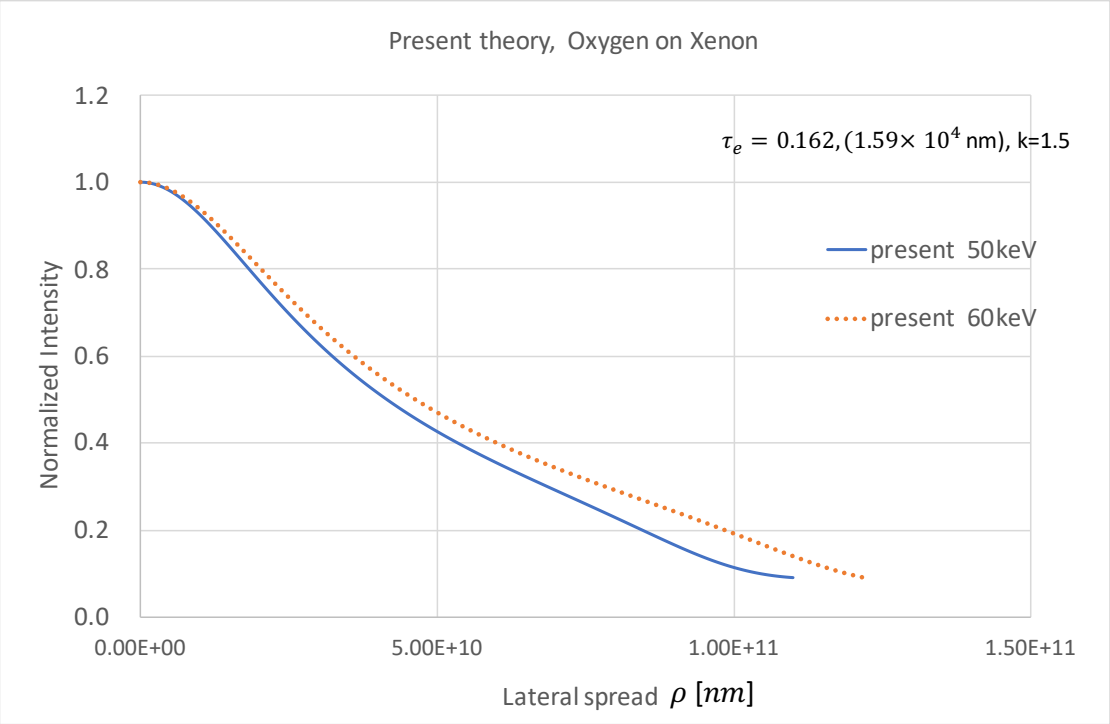
Present theory, Oxygen on Xenon
$\tau_e = 0.162, (1.59\times 10^4$ nm), k=1.5
present 50keV
present 60keV
Normalized Intensity
1.2
1.0
0.8
0.6
0.4
0.2
0.0
0.00E+00
5.00E+10
1.00E+11
1.50E+11
Lateral spread ρ $[nm]$

Fig. 4 (c)

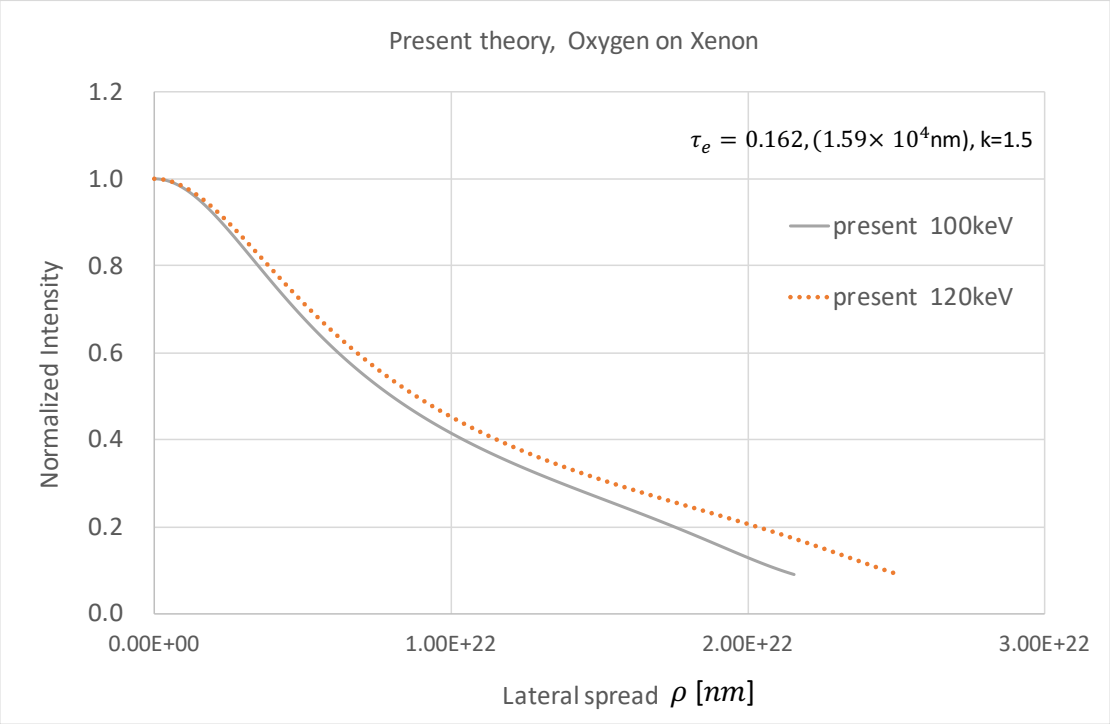
Present theory, Oxygen on Xenon
$\tau_e = 0.162, (1.59\times 10^4 \text{nm})$, k=1.5
present 100keV
present 120keV
Normalized Intensity
1.2
1.0
0.8
0.6
0.4
0.2
0.0
0.00E+00
1.00E+22
2.00E+22
3.00E+22
Lateral spread ρ $[nm]$

Fig. 5 (a)

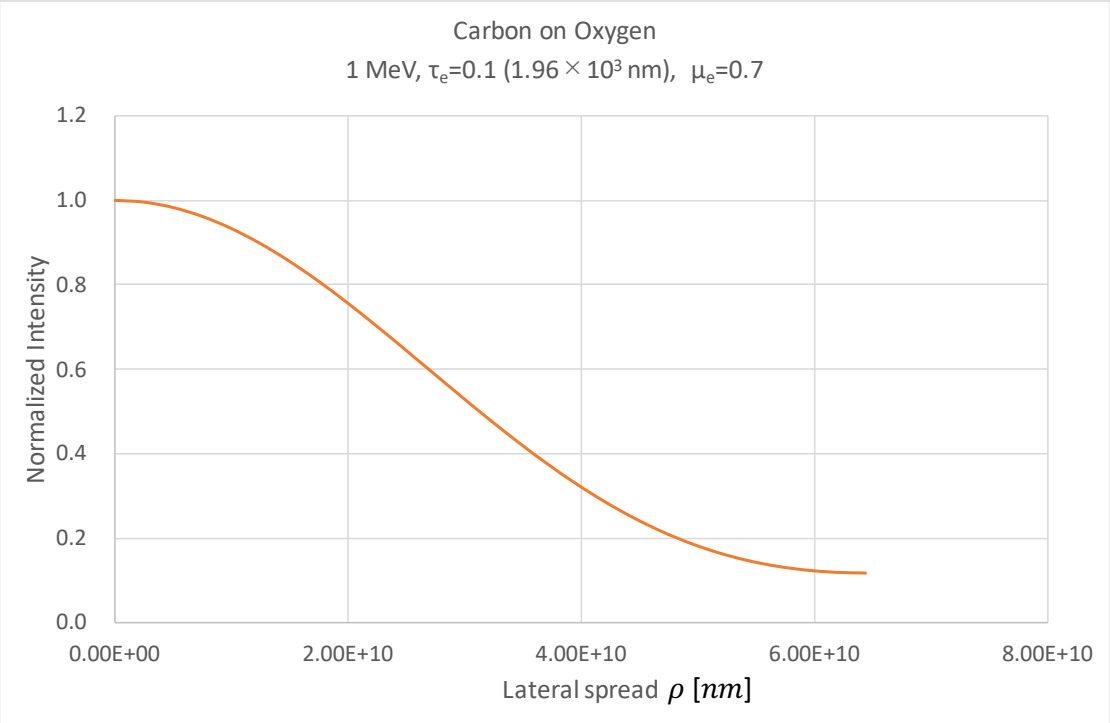
Carbon on Oxygen
1 MeV, τe=0.1 (1.96 × 10³ nm), μe=0.7
Normalized Intensity
1.2
1.0
0.8
0.6
0.4
0.2
0.0
0.00E+00
2.00E+10
4.00E+10
6.00E+10
8.00E+10
Lateral spread ρ [nm]

Fig. 5 (b)

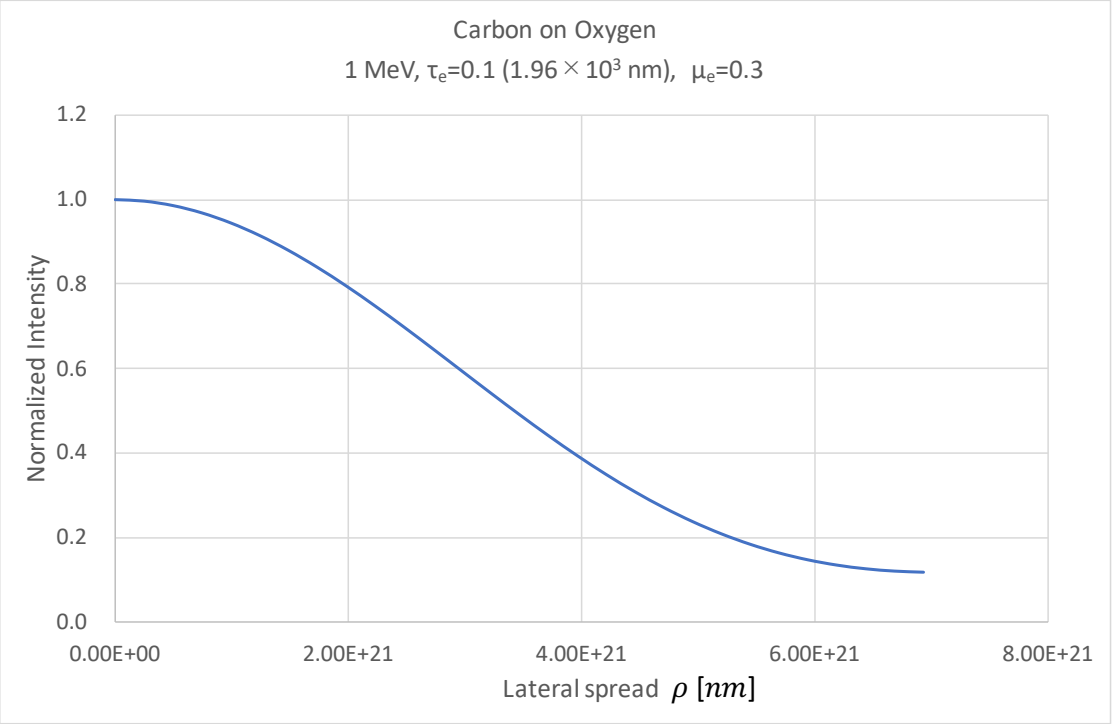
Carbon on Oxygen
1 MeV, τe=0.1 (1.96 × 10³ nm), μe=0.3
Normalized Intensity
1.2
1.0
0.8
0.6
0.4
0.2
0.0
0.00E+00
2.00E+21
4.00E+21
6.00E+21
8.00E+21
Lateral spread ρ [nm]

Fig. 5 (c)

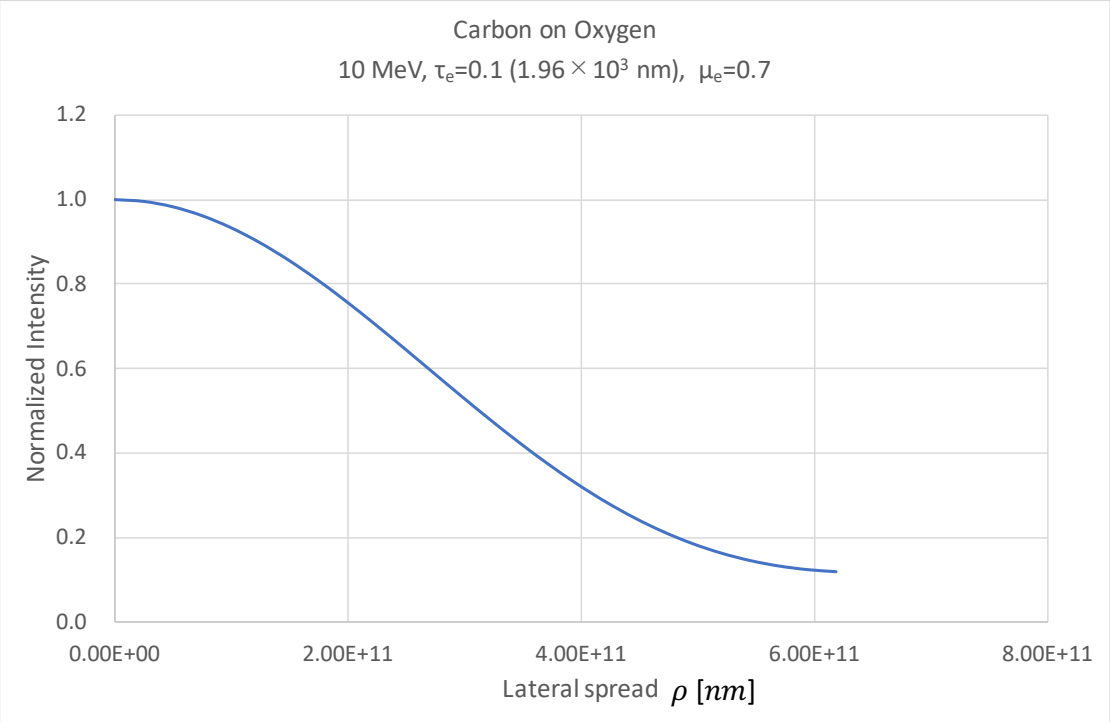
Carbon on Oxygen
10 MeV, τe=0.1 (1.96 × 10³ nm), μe=0.7
Normalized Intensity
1.2
1.0
0.8
0.6
0.4
0.2
0.0
0.00E+00
2.00E+11
4.00E+11
6.00E+11
8.00E+11
Lateral spread ρ [nm]

Fig. 5 (d)

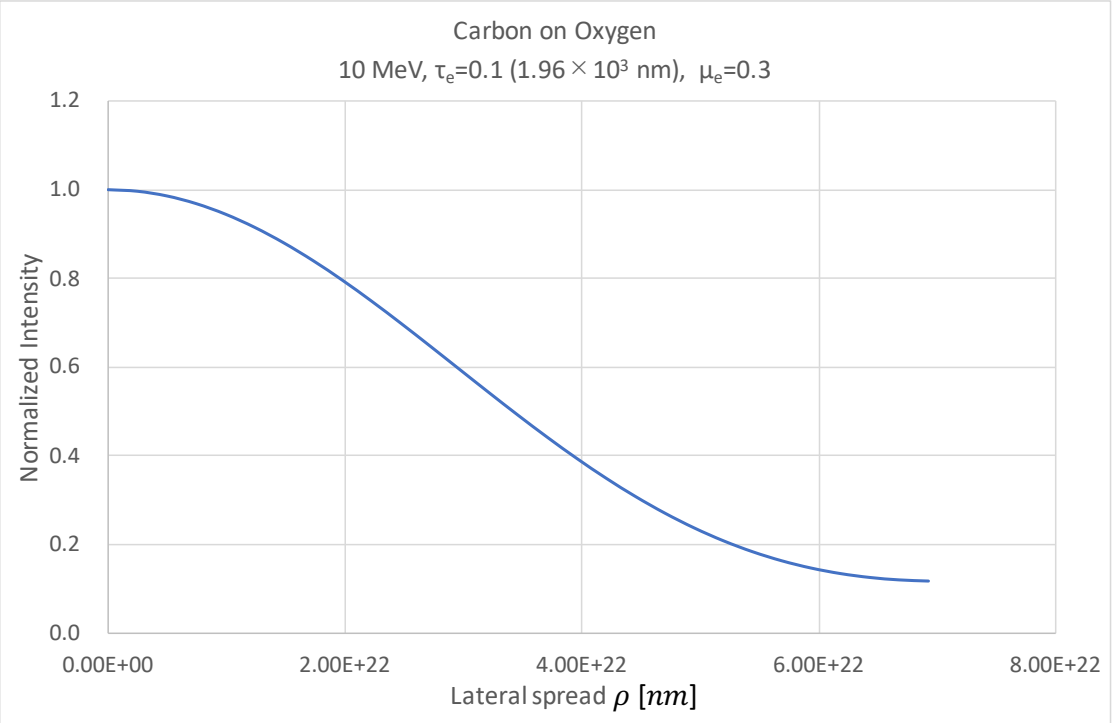
Carbon on Oxygen
10 MeV, τe=0.1 (1.96 × 10³ nm), μe=0.3
Normalized Intensity
1.2
1.0
0.8
0.6
0.4
0.2
0.0
0.00E+00
2.00E+22
4.00E+22
6.00E+22
8.00E+22
Lateral spread ρ [nm]

Fig. 6 (a)

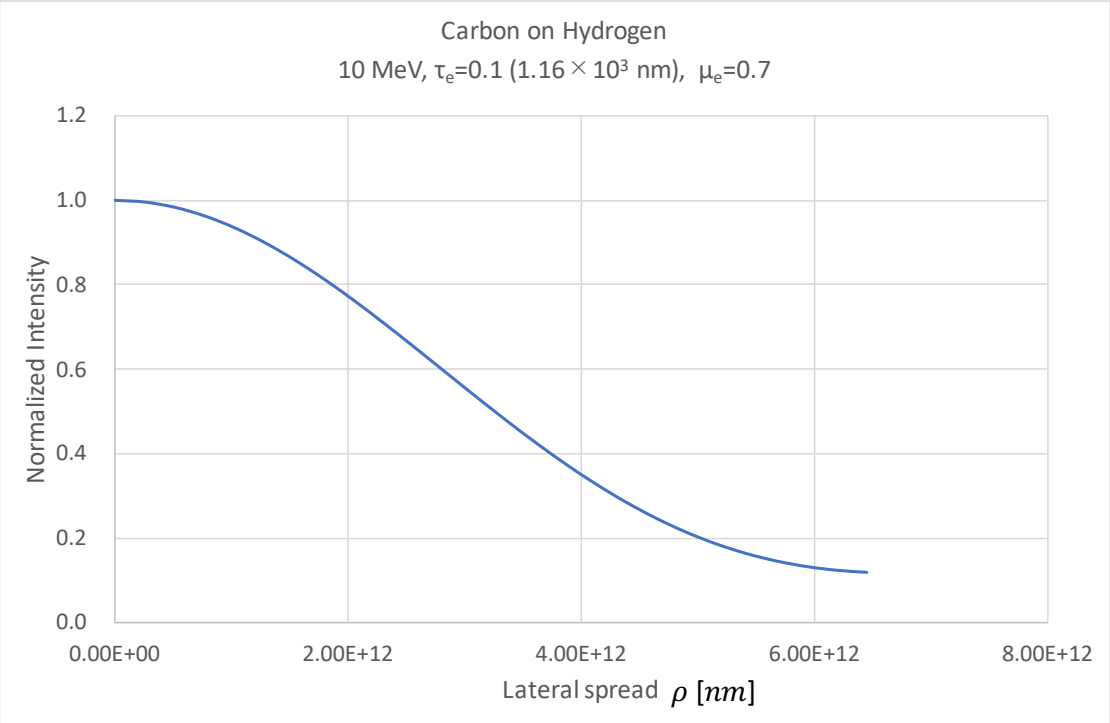
Carbon on Hydrogen
10 MeV, τe=0.1 (1.16 × 10³ nm), μe=0.7
Normalized Intensity
1.2
1.0
0.8
0.6
0.4
0.2
0.0
0.00E+00
2.00E+12
4.00E+12
6.00E+12
8.00E+12
Lateral spread ρ [nm]

Fig. 6 (b)

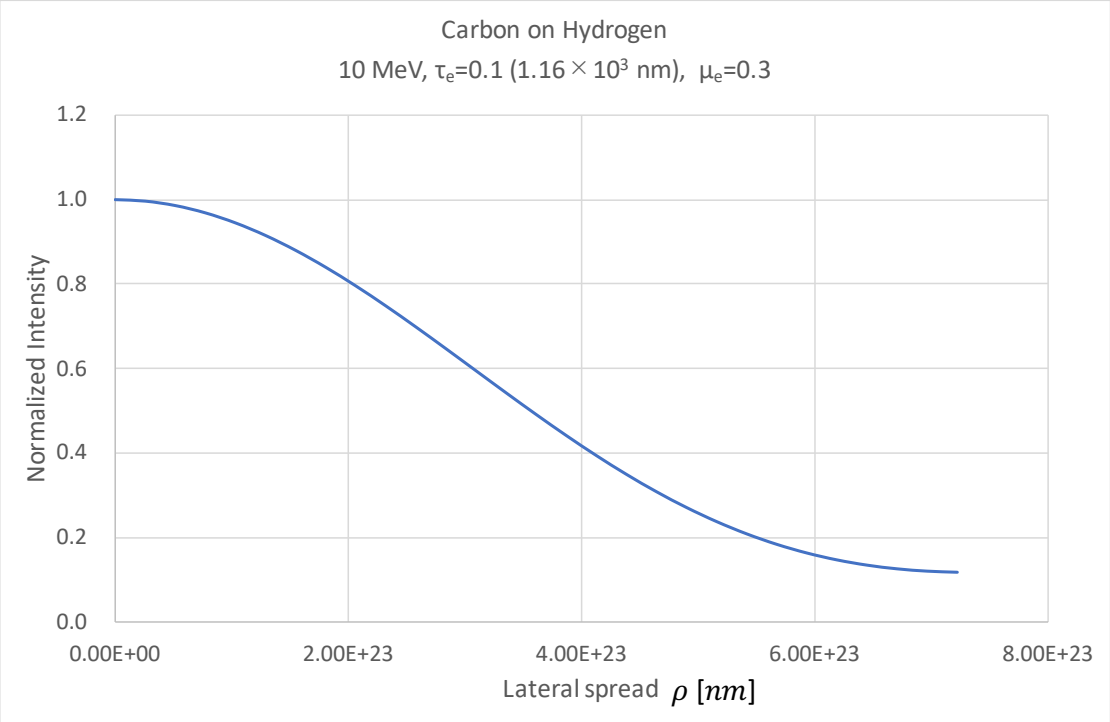
Carbon on Hydrogen
10 MeV, τe=0.1 (1.16 × 10³ nm), μe=0.3
Normalized Intensity
1.2
1.0
0.8
0.6
0.4
0.2
0.0
0.00E+00
2.00E+23
4.00E+23
6.00E+23
8.00E+23
Lateral spread ρ [nm]